Automatic Detection of Turning Points for Partial Trend Analysis in InSAR Deformation Time Series: EGMS Ortho Products

Rasoul Eskandari and Marco Scaioni

Abstract

Identifying turning points (TPs) in time series is essential for understanding changes in trend behaviour, especially in geodetic applications such as ground deformation monitoring. This study introduces a new automatic TP detection framework based on robust local regression models, specifically by contrasting Local Linear Regression (LLR) using Locally Weighted Scatterplot Smoothing (LOWESS) and Local Quadratic Regression (LQR) using Locally Estimated Scatterplot Smoothing (LOESS). The difference between these models is smoothed into a diagnostic signal, where extrema indicate potential TPs. A simulation-based calibration is developed to relate the prominence of each extremum to the magnitude and sign of gradient change, enabling both localisation and quantification of deformation transitions. The method is first validated using synthetic time series with known structural changes under varying noise and sample size conditions, demonstrating high accuracy in both TP positioning and gradient estimation. It is then applied to real-world InSAR deformation time series (DefTS) from the European Ground Motion Service (EGMS), confirming the method's ability to detect significant changes in displacement trends across both vertical and horizontal components. While sensitive to periodic behaviour and sudden jumps, the approach offers a promising step toward statistically grounded, automatic and interpretable TP detection in large-scale InSAR DefTS.

Keywords

Change point detection · Deformation time series (DefTS) · InSAR · Local regression models · Turning points

1 Introduction

Satellite Interferometric Synthetic Aperture Radar (InSAR) is a powerful, microwave remote sensing technology capable of providing dense, millimetric-precision measurements of ground surface motion over time. By processing stacks of SAR images, InSAR allows the generation of deformation time series (DefTS) that reveal both linear and non-linear trends in ground displacement (Ferretti et al. 2000). These non-linearities often contain turning points (TPs), locations in time where the trend direction or rate of deformation changes. Such TPs may arise due to a variety of causes, including landslide dynamics (Ghaderpour et al. 2024a), anthropogenic activities such as groundwater extraction or tunnelling (Samsonov et al. 2013), or environmental forcing (Eskandari and Scaioni 2024). Automatically detecting these TPs is of great importance for multiple reasons. It enhances early warning systems by signalling sudden shifts in surface behaviour, supports infrastructure risk assessment by pinpointing periods of accelerated movement, and contributes to long-term monitoring by enabling the segmentation and interpretation of complex deformation patterns.

R. Eskandari (✉) · M. Scaioni
Department of Architecture, Built Environment and Construction Engineering, Politecnico di Milano, Milan, Italy
e-mail: rasoul.eskandari@polimi.it

International Association of Geodesy Symposia,
https://doi.org/10.1007/1345_2026_368, © The Author(s) 2026

A variety of methods have been proposed in the literature for detecting TPs in time series (TS). A category of methods includes statistical tests and model-based inference approaches, which aim to identify structural changes using hypothesis testing or probabilistic models that infer shifts in the underlying process (Zuo et al. 2019; Madrid Padilla et al. 2021; Ardia et al. 2024). A second category comprises regression-based and piecewise models, where the TS is segmented into linear or polynomial trends, and TPs are estimated as breakpoints between segments (Raspini et al. 2018; Masiliūnas et al. 2021). More recently, a third class of methods has emerged based on deep learning techniques, where models such as recurrent neural networks or attention mechanisms are trained to recognize patterns associated with trend reversals (Lattari et al. 2022; Shahryarinia et al. 2025; Arya Fakhri and Satari 2025), often requiring large labeled datasets and computational resources.

Within regression-based approaches, recent methods have been specifically developed for TP detection in InSAR deformation measurements. For instance, the sequential turning point detection (STPD) method identifies TPs by fitting piecewise linear trends within moving windows and testing slope differences, while incorporating an adaptive windowing strategy to reduce sensitivity to seasonal effects (Ghaderpour et al. 2024b). A dedicated metric, namely normalized difference residual index, is also introduced to distinguish true TPs from abrupt jumps. The approach has been successfully applied to real-world InSAR DefTS (Ghaderpour et al. 2024c,d). Similarly, the running slope difference (RSD) method detects TPs by statistically comparing slopes of adjacent segments using a t-test formulation (Zuo et al. 2019). While effective and interpretable, its performance depends on window selection and can be sensitive to noise and sampling characteristics.

Building on these previous efforts, this study introduces a novel, fully automated approach for automatically detecting TPs in TS using robust local regression models. The proposed method exploits the contrast between local linear and quadratic fits to identify significant changes in slope, representing potential TPs, without the need for manual segmentation or predefined model structures. Through simulation experiments, the method is validated for its ability to localize multiple TPs accurately and to quantify the associated gradient modifications in both magnitude and sign. Its applicability is further demonstrated on real-world InSAR-derived DefTS from the European Ground Motion Service (EGMS) (Costantini et al. 2022), confirming its potential as a reliable and interpretable framework for automatic detection of meaningful deformation transitions.

2 Methodology

This study introduces a fully automated method for detecting TPs in univariate TS, based on the local curvature difference between two robust local regression models. The method contrasts local linear regression (LLR) and local quadratic regression (LQR), capturing points of significant slope change through a smooth diagnostic vector, denoted $\gamma(t)$. TPs are detected as extrema in γ, with their position and prominence directly linked to both the location and value of the underlying gradient change (ΔG).

Two robust local regression techniques are applied to the TS: Locally Weighted Scatterplot Smoothing (LOWESS) and Locally Estimated Scatterplot Smoothing (LOESS) (Gijbels and Prosdocimi 2010; Sharma et al. 2015), which are respectively called LLR and LQR models hereafter. LLR fits a local linear model to capture the first-order trend, while LQR fits a local quadratic model to additionally capture curvature. Both models are fitted using a robust procedure involving kernel-based weighting and iterative reweighting to reduce the influence of outliers. The window size for both models is defined as $h = 6\sqrt{N}$, where N is the total number of TS samples.

The window sizes adopted for the local regression models and for the moving-average smoothing (as discussed later) were selected empirically to provide a balance between capturing meaningful local trend changes and avoiding oversensitivity to short-term fluctuations caused by noise, especially for the sample sizes commonly encountered in InSAR DefTS. In the present implementation, both windows are defined as functions of the total number of samples, so that the smoothing remains adaptive to TS length. Nevertheless, these parameters could also be tuned according to the expected noise level, sampling characteristics, and other properties of the analysed series.

2.1 TP Detection: Local Curvature Contrast

Let the input TS be denoted by $y(t)$, observed over $t = 1, \ldots, N$. Two robust local regression models are fitted: a local linear regression $\hat{y}^{LLR}(t)$ and a local quadratic regression $\hat{y}^{LQR}(t)$, each applied over a moving window of size $6\sqrt{N}$.

The difference between these two fitted trends highlights local curvature, with deviations most prominent near structural changes in the slope. To stabilise the resulting contrast and suppress local fluctuations, a moving average (MA) is applied over a window of length $2\sqrt{N}$, yielding the

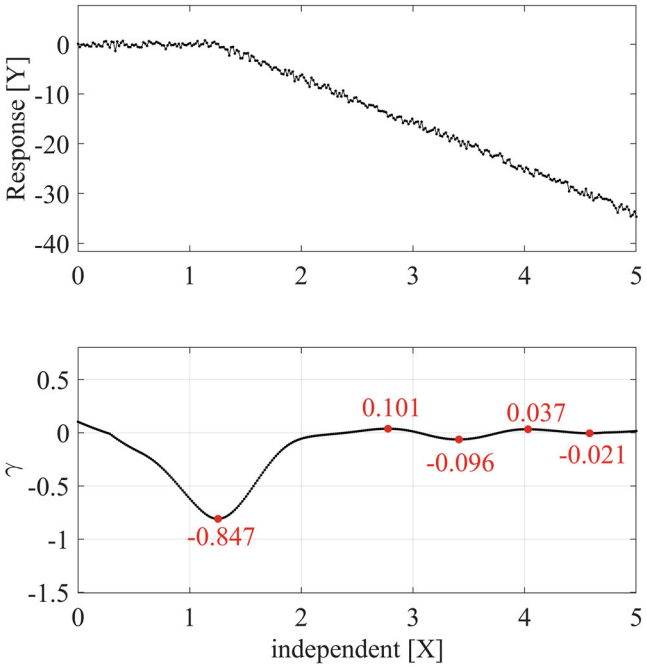

Fig. 1 Simulated time series with the presence of a turning point (above), and corresponding gamma behaviour with detected extremum points and their prominence (below)

diagnostic signal

$$\gamma(t) = MA\left(\hat{y}^{LLR}(t) - \hat{y}^{LQR}(t)\right) \tag{1}$$

As illustrated in Fig. 1, this smoothed curvature signal $\gamma(t)$ exhibits a clear and dominant extremum near the location of the imposed TP, with $\Delta G = 9$ arbitrary unit of slope, in the simulated TS (top panel of Fig. 1). This prominent dip corresponds to a significant change in the slope of the underlying trend and is well separated from other minor extrema that may result from noise or weak local fluctuations.

The extremum's position aligns with the location of the turning point, while its prominence reflects the strength of the local gradient change. In this example, the deepest extremum reaches approximately -0.85, standing out distinctly from smaller peaks and valleys, which are not indicative of meaningful structural changes. This observation supports the hypothesis that both the location and size of a TP can be inferred directly from the position and prominence of extrema in $\gamma(t)$. In the example demonstrated in Fig. 1, a relatively low noise level is considered to clearly illustrate the effect of a TP in the TSs. More challenging scenarios with higher noise levels are investigated in the simulation experiments presented in Sect. 3.

2.2 Prominence-Gradient Calibration Model

To quantify the relationship between the prominence of detected extrema (Ext_{Prom}) and the underlying gradient change ΔG, a comprehensive simulation study was conducted. The objective was to construct predictive models that allow (*i*) estimation of the minimum prominence required to signify a meaningful change in slope, and (*ii*) retrieval of the size of ΔG from a measured prominence. A total of 10,000 synthetic TSs were generated, each containing a known TP located at the centre of the series. The simulated data are expressed in arbitrary unit (a.u.) of observation (e.g., deformation in mm), and time is represented as a generic time variable (e.g., year). Accordingly, slope values are reported in a.u./time.

These simulations spanned a wide range of configurations: N:50–500 timestamps, imposed ΔG: -20 to 20 a.u./time, initial slope (first part of the simulated TS): -50 to 50 a.u./time, and Gaussian noise standard deviation: 0.1–3 a.u. For each series, the diagnostic vector $\gamma(t)$ was computed, and the prominence of the extremum in the vicinity of the true TP was recorded as Ext_{Prom}.

The resulting data revealed a strong and interpretable structure, as shown in Fig. 2. In the top panel, a clear positive correlation is observed between the imposed ΔG and the resulting Ext_{Prom}. This relationship is tighter for larger sample sizes (indicated by reddish colours), confirming that longer TS enable more confident detection of TPs. Conversely, smaller sample sizes lead to increased variability, but the general trend remains monotonic. In the bottom panel of Fig. 2, a similar behaviour can be observed within a different domain. Notably, the sign of the prominence reflects the direction of change (increasing or decreasing slope), not just the magnitude, making the model capable of estimating both the value and sign of the ΔG.

Based on this simulation set, two Gaussian Process Regression (GPR) models were developed. The first model, denoted as M^1_{thresh}, maps a given pair (N, ΔG^*) to a threshold prominence $Prom_{thresh}$, enabling detection of statistically significant extrema that correspond to a user-defined gradient change ΔG^*. The second model M^2_{thresh} performs the inverse operation by mapping (N, Ext_{Prom}), estimating the underlying gradient change $\overline{\Delta G}$ directly from the observed prominence and TS length. The coefficient of determination (R^2) of the GPR operation for both developed models is approximately 0.94.

Despite of N, no correlation has been found in the behaviour of ΔG and Ext_{Prom} with the level of noise imposed

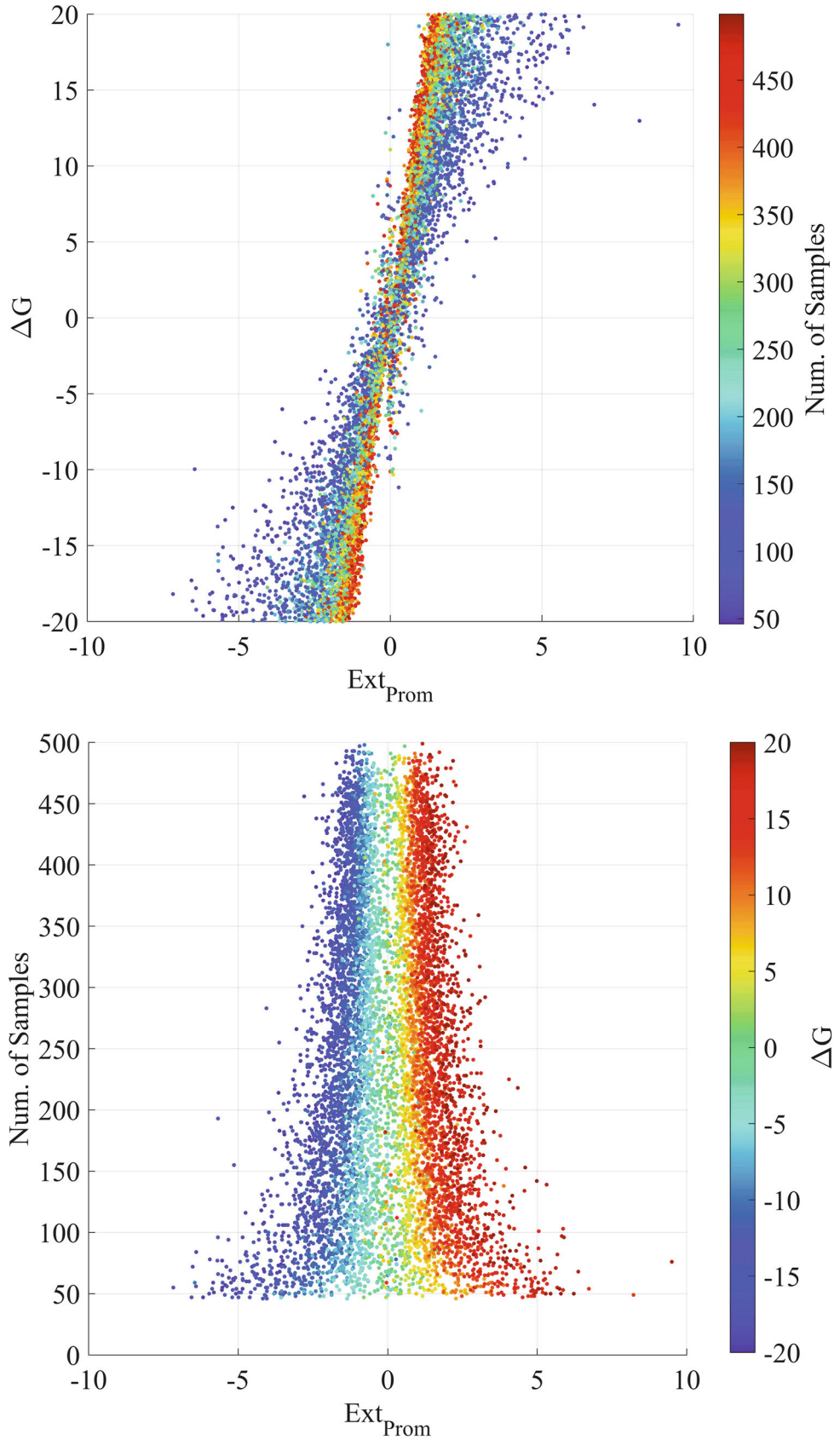

Fig. 2 Correlation between number of samples (N), gradient change (ΔG) and prominence of detected extremum (Ext_{Prom})

on each simulated TS or with the initial slope (the first part of the simulated TS), therefore, these have not been considered as independent variables in the GPR modelling.

Together, these models form a calibrated framework for automatic TP detection. By comparing detected prominences against $Prom_{thresh}$, the method filters out spurious extrema caused by noise, retaining only those likely to reflect significant structural changes. For each retained TP, its location is given by the extremum position in $\gamma(t)$, while its gradient change is estimated using M^2_{thresh}, including the sign. This dual capability ensures that the method not only locates TPs accurately but also provides insight into the intensity and direction of change, essential for interpreting dynamics in complex TS.

2.3 Non-TP Influences in γ Dynamics

While TPs manifest as distinct extrema in the diagnostic signal γ, they are not the only structural elements that can induce such behaviour. In particular, abrupt discontinuities (i.e., jumps) and periodic or oscillatory patterns (e.g., seasonality) may also generate significant extrema in γ, potentially leading to false detections if not interpreted carefully. As shown in Fig. 3, a simulated TS containing a sharp jump (equal to -2π a.u.) in level near the midpoint produces a prominent peak in γ, even though the local slope before and after the jump remains unchanged. This occurs because

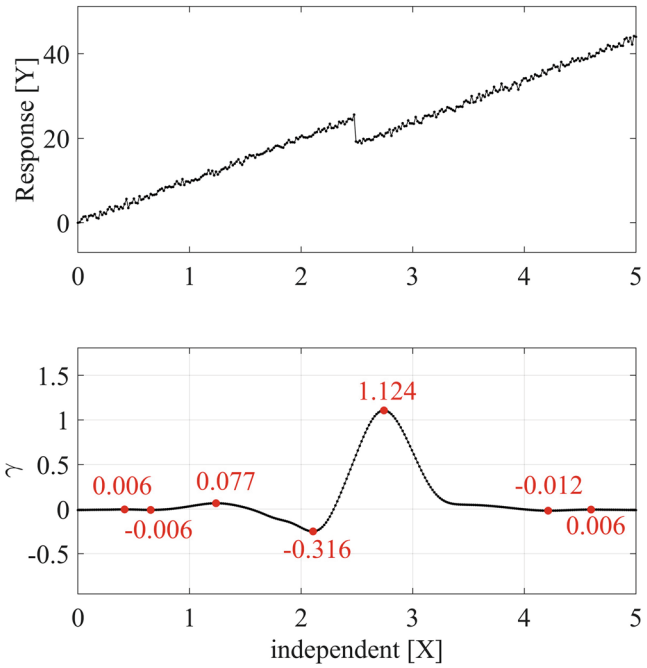

Fig. 3 Effect of the presence of a discontinuity point (jump) on diagnostic vector γ

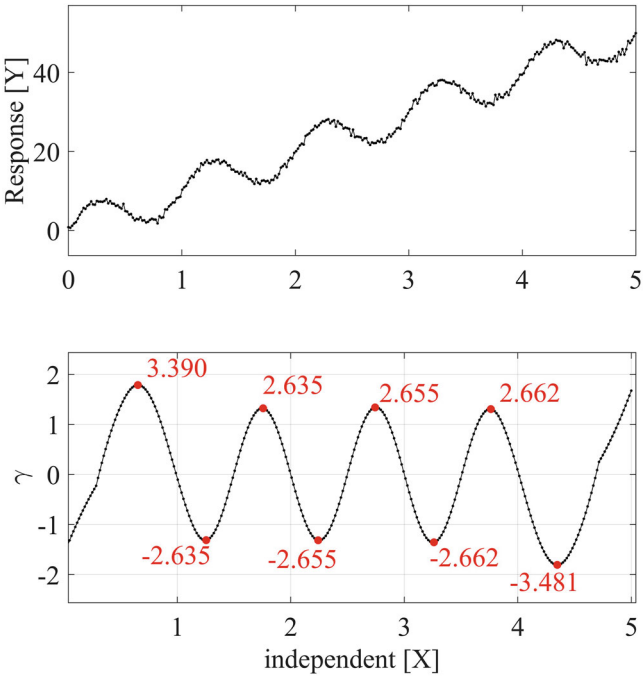

Fig. 4 Effect of the presence of high-frequency fluctuations (seasonality) on diagnostic vector γ

both LLR and LQR attempt to smooth the abrupt change, leading to a large residual curvature in the vicinity of the jump. The LQR tends to overshoot near the discontinuity, while the LLR underfits, resulting in a sharp positive contrast and a high-prominence extremum. However, this does not represent a true TP in the trend's slope; it reflects a structural break in level, not gradient.

Similarly, Fig. 4 illustrates the behaviour of γ in the presence of a seasonal pattern (with an amplitude of 3 a.u.). Here, the cyclic structure introduces repeated high-amplitude peaks and valleys, even though no permanent change in slope direction exists. This results from the curvature imposed by the periodic nature of the signal: as the direction of the local trend oscillates, so does the difference between LQR and LLR fits, creating regular extrema in γ. These are not necessarily errors, but rather expected responses to strong oscillatory behaviour, and should be interpreted differently from structural TPs in the long-term trend.

Unlike approaches such as STPD (Ghaderpour et al. 2024b), which incorporate specific mechanisms to distinguish jumps from true turning points and can operate under the presence of seasonal components, the proposed method assumes that such effects are either negligible or mitigated prior to analysis. This assumption allows a simpler and fully automated framework, while focusing on detecting changes in the underlying trend curvature. To ensure accurate and automatic detection of true TPs, components such as jumps and seasonal patterns should be carefully identified and

removed from the TS prior to analysis. These features can introduce high-prominence extrema in the diagnostic γ that do not correspond to actual changes in the slope of the underlying trend, thereby acting as false positives in the detection process.

In contrast, other irregularities, such as random noise and isolated outliers, do not pose the same level of threat to the method's integrity. This is due to the use of robust local regression models, i.e., LLR and LQR, which incorporate iterative reweighting schemes to reduce the influence of anomalous data points. As a result, the outliers are naturally downweighted, and their impact on the fitted curves (and hence on γ) is minimised. Furthermore, the simulation study presented in Sect. 2.2 confirms that the method maintains consistent detection behaviour across a wide range of noise levels, reinforcing its resilience in noisy or imperfect datasets.

The proposed framework assumes a uniformly sampled time vector for the input TS. Nevertheless, it has been observed in a separate analysis that a limited proportion of missing samples, up to approximately 10%, randomly distributed along the series, does not significantly affect the TP detection capability of the method. This is mainly due to the smoothing nature of the local regression models. More structured or larger gaps may require preprocessing (e.g., interpolation), and this will be investigated in future work.

3 Results on Simulated Dataset

To evaluate the performance of the proposed method under controlled conditions, a synthetic TS of length $N = 300$ was generated with a Gaussian noise level of 1 a.u. Two isolated outliers are also added to TS to demonstrate the ability of the method in discarding this kind of irregularities. Two distinct changes in slope, representing actual TPs, were imposed at known locations: a positive ΔG of $+5$ a.u./time near the first quarter and a negative ΔG of -10 a.u./time near the last quarter of the series. These transitions occur at the 75th and 225th timestamps, respectively, as indicated by vertical lines in the upper panel of Fig. 5.

Following the methodology, robust LLR and LQR models were applied, and the smoothed curvature difference vector γ was computed, and local extrema were extracted. A significance threshold for gradient detection was defined as $\Delta G^* = \pm 3$ a.u./time only for illustrative purposes. Using the calibration model M^1_{thresh} $(N, \Delta G^*)$, the corresponding prominence thresholds were obtained: $+0.307$ and -0.294 a.u. for positive and negative significant changes, respectively. Extrema exceeding these thresholds in absolute value were retained as valid TPs.

In this example, two prominent extrema were identified: one with Ext_{Prom} equal to $+0.466$ a.u. and another with -1.025 a.u., both surpassing their respective thresholds. For these two detected TPs, the estimated ΔG were $+4.666$ and -9.563 a.u./time using model M^2_{thresh} (N, Ext_{Prom}). These estimates are remarkably close to the true ΔG of $+5$ and -10 a.u./time, demonstrating strong agreement in both magnitude and sign. Furthermore, the estimated positions (78 and 226) are within 3 samples of the actual turning points (75 and 225), confirming high temporal precision of the method.

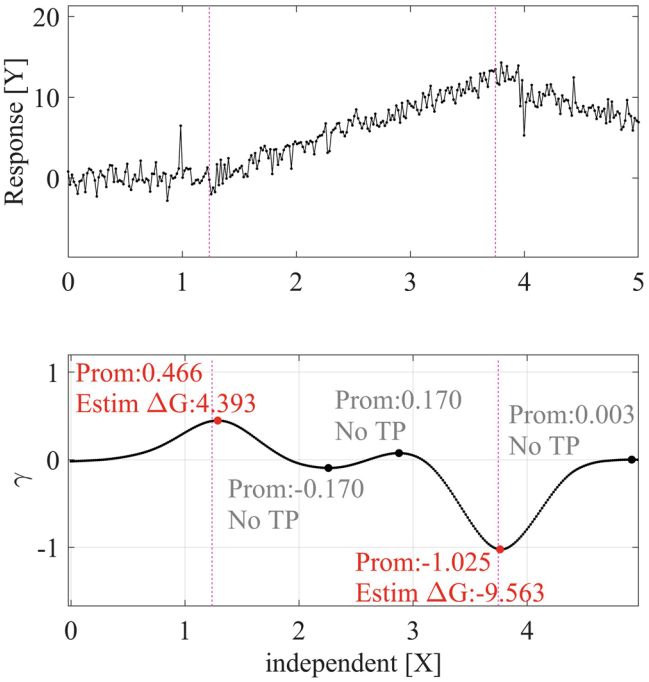

Fig. 5 Example 1: The actual TPs on simulated TS (above) and detected TPs with position and estimated gradient change (below)

As also shown in the bottom panel of Fig. 5, other local extrema in the γ vector were correctly discarded as non-significant, based on the selected threshold. This example illustrates the ability of the method to accurately detect both the presence and scale of significant TPs, while rejecting noise-induced fluctuations.

To further evaluate the robustness of the proposed method, a second simulation was conducted using a TS of length $N = 150$ and a noise level of 2 a.u., representing a more challenging scenario with fewer observations and greater variability (see Fig. 6). In this setup, the underlying slope begins at -10 a.u./time, changes to $+5$ a.u./time around the second third of the TS and reverts to -10 a.u./time near the end. These transitions correspond to two TPs, each with true ΔG of 15 a.u./time.

After applying robust LLR and LQR smoothing and computing the diagnostic γ, the extrema were extracted. Two prominent extrema were detected with estimated ΔG of $+18.87$ and -18.29 a.u./time, with true values of $+15$ and -15 a.u./time, respectively. The true positions of the TPs

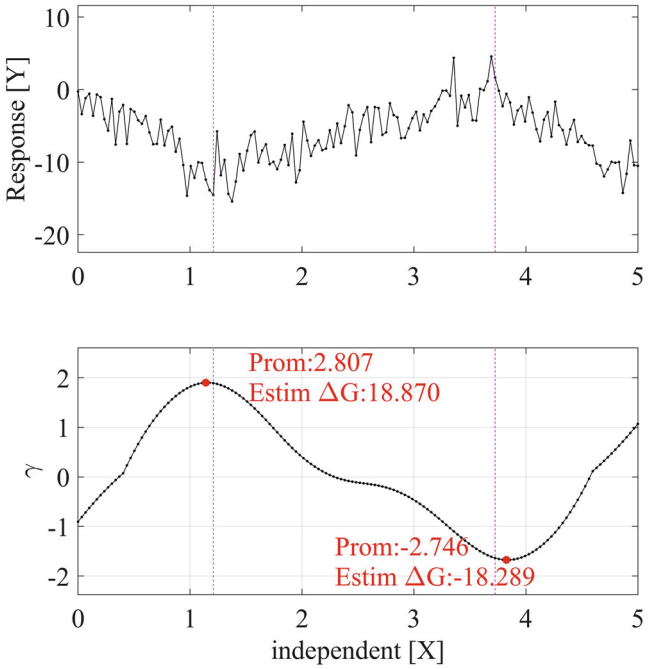

Fig. 6 Example 2: The actual TPs on simulated TS with low N and high noise level (above) and detected TPs with position and estimated gradient change (below)

were set at timestamps 37 and 112 (purple lines in Fig. 6), while the estimated positions of these extrema were found at timestamps 35 and 115, which are within only 2–3 samples of the actual TPs, confirming strong temporal accuracy even under noisy conditions.

As shown in Fig. 6, the diagnostic signal remains well-structured despite the high noise level, and the estimated ΔG values remain consistent in both magnitude and sign with the true transitions. This example demonstrates the ability of the method to reliably detect significant TPs even when data quality is limited, further confirming the effectiveness of the procedure across varying conditions of sample size and noise.

Compared to methods such as STPD (Ghaderpour et al. 2024b), which rely on piecewise linear modelling and residual minimisation within moving windows, the proposed approach captures TPs through local curvature differences between regression models. This enables a direct link between detected extrema and gradient change magnitude, while maintaining robustness under varying noise levels, as demonstrated in the simulations.

4 Results: Real-World InSAR DefTS

To demonstrate the practical applicability and performance of the automatic TP detection framework, real-world geodetic DefTS derived from InSAR observations are analysed. Specifically, datasets from the EGMS are utilised for this purpose.

The EGMS is a continental-scale Earth observation initiative provided by the Copernicus Land Monitoring Service (CLMS) (https://land.copernicus.eu/), offering standardised, open-access ground motion products derived from Sentinel-1 SAR data using Persistent Scatterer Interferometry (PSI) (Costantini et al. 2022). These products represent millimetric DefTS of the Earth's surface across Europe over time, and are intended for applications in geohazard monitoring (Marmoni et al. 2025), infrastructure stability (Eskandari and Scaioni 2025a), urban subsidence (Antoniadis et al. 2023), and other geodynamic studies (Eskandari and Scaioni 2025b).

EGMS data are made available in several product levels, including Basic and Calibrated on the sparse grid of Sentinel-1 resolution, and Ortho products on a 100-m spatial resolution. In this study, the analysis is conducted on the Ortho-level products, specifically the Up-Down (U-D) and East-West (E-W) components (obtained from the dataset titled as EGMS-Ortho-E44N25-2019_2023, extracted from https://egms.land.copernicus.eu/), which covers the period 2019–2023 with a nominal temporal resolution of 6 days.

The subsequent discussion illustrates the application of the proposed detection method to DefTS extracted from this dataset, highlighting its capability to automatically identify meaningful changes in ground motion behaviour. For illustrative purposes, a representative threshold of $\Delta G =$ 3 mm/year is used to highlight the detection of meaningful changes. This parameter is user-defined and can be adjusted depending on the application and noise characteristics of the dataset.

For the U-D DefTS (Fig. 7), two distinct turning points are identified. These correspond to periods where the vertical ground motion shifts noticeably, with estimated ΔG of approximately -3.5 and $+3.5$ mm/year, with prominence values of -0.38 and $+0.38$ mm, respectively. The symmetry of these values suggests a transition from a relatively stable deformation trend to a more accelerated subsidence phase, followed by a recovery or deceleration, clearly visible in the deformation signal.

Similarly, the E-W component (Fig. 8) exhibits a significant extremum in the γ signal, with a prominence of 0.34 mm, and an associated estimated $\Delta G = 3.24$ mm/year. This indicates a lateral shift in surface displacement trends occurring around the same period observed in the U-D component.

There is an extremum point in E-W, approximately at the position of the second TP in the U-D case, which is not detected as TP, which may be due to the low prominence value in extremum detection. Notably, the timing of the detected TPs is consistent across both directional components, suggesting a coherent deformation process affecting

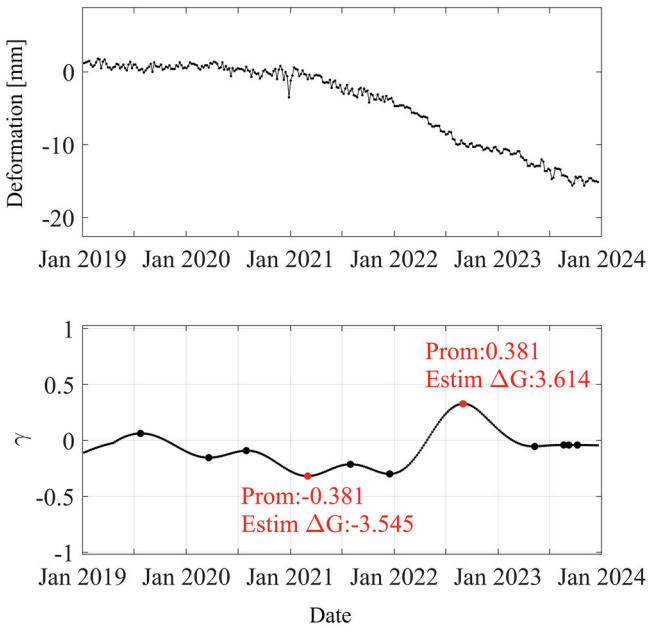

Fig. 7 EGMS U-D deformation time series (above) and detected TPs (below)

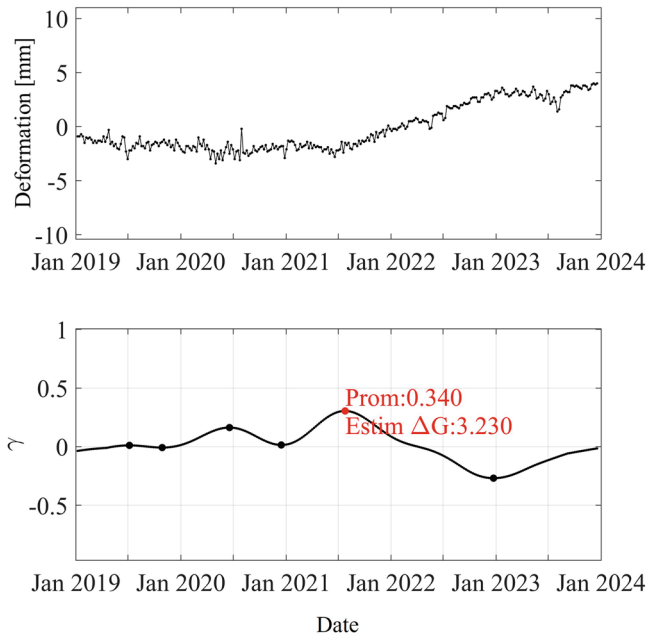

Fig. 8 EGMS E-W deformation time series (above) and detected TPs (below)

both vertical and horizontal motion. The fact that these transitions are clearly detected and quantified in both components reinforces the effectiveness of the method in identifying meaningful kinematic changes within real-world InSAR-derived DefTS.

The proposed method involves computationally lightweight operations, including local regression fitting and extremum extraction, which are expected to be efficient for processing large numbers of measurement points, particularly in wide-area applications using EGMS. Some TP detection approaches, such as STPD, also have demonstrated efficient performance for large-scale InSAR DefTS analysis. However, a quantitative comparison with other TP detection methods, in terms of both computational time and detection accuracy, will be addressed in future work.

5 Conclusions

This study presented a novel method for the automatic detection of TPs in univariate TS, based on the behaviour of robust local regression models. The approach relies on the contrast between LLR (using LOWESS) and LQR (using LOESS), computed over adaptive window sizes, with their difference smoothed into a diagnostic signal γ. TPs are identified as prominent extrema in γ with prominence values calibrated through a simulation-based model to assess both significance and gradient change magnitude. The method is capable of capturing multiple gradient modifications throughout the TS, and it provides an estimate of the position and size of those TPs.

The method was first validated on simulated TS, designed with known structural changes and varying noise levels. Results confirmed that the method accurately identified the locations of imposed TPs and estimated the associated gradient changes with high precision, even under low sample sizes or elevated noise conditions. Following this, the technique was applied to real-world InSAR-derived DefTS from the EGMS. In both the U-D and E-W components, the method successfully detected key transitions in ground motion, confirming its practical value in large-scale geodetic monitoring. Several important characteristics were demonstrated:

- The method is fully automated, requiring only the TS and a user-defined threshold for significant gradient change.
- It is robust to noise and outliers, owing to the use of robust local regression.
- The estimated TPs provide both temporal location and an interpretation of motion dynamics via the estimated signed gradient change.

This work represents an initial investigation into the potential of local regression models for unsupervised TP detection. While promising, the method also has limitations, particularly its sensitivity to seasonal behaviour (high-frequency fluctuations) and sudden level shifts (jumps), which may induce false positives in γ signal. Nevertheless, the results highlight the value of the underlying idea and establish a foundation for future work. Extensions may explore more advanced statistical frameworks, such as adaptive detrending, signal decomposition to enhance robustness and extend the method to more complex or multivariate TS applications.

Competing Interests The author(s) has no competing interests to declare that are relevant to the content of this manuscript.

References

Antoniadis N, Alatza S, Loupasakis C, Kontoes C (2023) Land subsidence phenomena vs. coastal flood hazard—the cases of messolonghi and Aitolikon (Greece). Remote Sens 15(8):2112

Ardia D, Dufays A, Ordás Criado C (2024) Linking frequentist and bayesian change-point methods. J Bus Econ Stat 42(4):1155–1168

Arya Fakhri S, Satari M (2025) Trend change point detection in InSAR derived displacement time series using MALkCNN: a deep learning approach. PFG—J Photogram Remote Sens Geoinform Sci 93(4):335–350

Costantini M, Minati F, Trillo F, Ferretti A, Passera E, Rucci A, Dehls J, Larsen Y, Marinkovic P, Eineder M, Brcic R, Siegmund R, Kotzerke P, Kenyeres A, Costantini V, Proietti S, Solari L, Andersen HS (2022) EGMS: Europe-wide ground motion monitoring based on full resolution InSAR processing of all Sentinel-1 acquisitions. In: Proceedings of IEEE international geoscience and remote sensing symposium IGARSS, pp 5093–5096

Eskandari R, Scaioni M (2024) Spatiotemporal pattern detection of ground deformations induced by extreme rainfall using InSAR EGMS: the case of Cortina d'ampezzo after Vaia storm. In: ISPRS annals of the photogrammetry, remote sensing and spatial information sciences, X-3-2024, pp 131–138

Eskandari R, Scaioni M (2025a) Joint use of EGMS and CosmoSkyMed InSAR for assessment of ground and structural deformations: the case of Como, northern Italy. In: Proceedings of 6th joint international symposium on deformation monitoring (JISDM), 1000180536

Eskandari R, Scaioni M (2025b) InSAR EGMS for wide-area assessment of extreme rainfall-related modifications of ground-deformation patterns: the case of Vaia rainstorm. In: Geomat Green Digital Transit, vol 2463, pp 46–60

Ferretti A, Prati C, Rocca FJIT, Sensing R (2000) Nonlinear subsidence rate estimation using permanent scatterers in differential SAR interferometry. IEEE Trans Geosci Remote Sens 38(5):2202–2212

Ghaderpour E, Masciulli C, Zocchi M, Bozzano F, Scarascia Mugnozza G, Mazzanti P (2024a) Estimating reactivation times and velocities of slow-moving landslides via PS-InSAR and their relationship with precipitation in Central Italy. Remote Sens 16(16):3055

Ghaderpour E, Antonielli B, Bozzano F, Scarascia Mugnozza G, Mazzanti P (2024b) A fast and robust method for detecting trend turning points in InSAR displacement time series. Comput Geosci 185:105546

Ghaderpour E, Mazzanti P, Bozzano F, Scarascia Mugnozza G (2024c) Ground deformation monitoring via PS-InSAR time series: an industrial zone in sacco river valley, Central Italy. Remote Sens Appl: Soc Environ 34:101191

Ghaderpour E, Antonielli B, Bozzano F, Scarascia Mugnozza G, Mazzanti P (2024d) Detecting trend turning points in PS-InSAR time series: slow-moving landslides in province of frosinone, Italy. Engineering Proceedings 68(1):12

Gijbels I, Prosdocimi I (2010) Loess. WIREs Comput Stat 2(5):590–599

Lattari F, Rucci A, Matteucci M (2022) A deep learning approach for change points detection in InSAR time series. IEEE Trans Geosci Remote Sens 60:1–16

Madrid Padilla OH, Yu Y, Wang D, Rinaldo A (2021) Optimal nonparametric change point analysis. Electr J Stat 15(1):1154–1201

Marmoni GM, Antonielli B, Caprari P, Di Renzo ME, Marini R, Mastrantoni G, Mazzanti P, Patelli D, Bozzano F (2025) Semi-automatic ranking of landslide candidate areas at a regional scale using EGMS InSAR data for territorial planning and risk management. Landslides 22(12):4077–4095

Masiliūnas D, Tsendbazar N-E, Herold M, Verbesselt J (2021) BFAST lite: a lightweight break detection method for time series analysis. Remote Sens 13(16):3308

Raspini F, Bianchini S, Ciampalini A, Del Soldato M, Solari L, Novali F, Del Conte S, Rucci A, Ferretti A, Casagli N (2018) Continuous, semi-automatic monitoring of ground deformation using Sentinel-1 satellites. Sci Rep 8(1):7253

Samsonov S, d'Oreye N, Smets B (2013) Ground deformation associated with post-mining activity at the french–german border revealed by novel InSAR time series method. Int J Appl Earth Obs Geoinf 23:142–154

Shahryarinia K, Omidalizarandi M, Heidarianbaei M, Sharifi MA, Neumann I (2025) Detecting change points in time series of InSAR persistent scatterers using deep learning models. Appl Geomat 17(2):357–366

Sharma S, Swayne DA, Obimbo C (2015) Automating the smoothing of time series data. Journal of Environmental and Analytical Toxicology 5(5):304

Zuo B, Li J, Sun C, Zhou X (2019) A new statistical method for detecting trend turning. Theor Appl Climatol 138(1):201–213